

Real-time prediction of unidirectional irregular waves

David Skene^{1,†}, Hugh Wolgamot¹, Justin Geldard¹, Paul Taylor,¹ and Scott Draper¹

¹The University of Western Australia, WA 6009, Australia, [†]david.skene@uwa.edu.au

Introduction

In recent years a substantial amount of literature has emerged on active control of wave energy converters (WECs) (see e.g. the review of Ringwood *et al.*, 2014). This work has indicated that a device’s power generation can be more than doubled if a WEC is actively controlled in response to the wave induced excitation force (Babarit & Clément, 2006; Ringwood *et al.*, 2014). By assuming linear hydrodynamics, it has also been shown by Falnes (1995) that in order to determine this excitation force the free surface of the water at the WEC’s location needs to be known into the future (as the free surface does not directly cause the excitation force, but becomes approximately causal if the free surface is known into the future).

It was proposed by Falnes (1995) that the way to make this prediction is to take up-wave measurements and make down-wave forecasts using the waves’ dispersive spatial-temporal relationship. This concept has since been fully realised by Qi *et al.* (2018), who were able to reconstruct synthetic and experimental surface gravity wave-fields surrounding a measurement location using a predictor-corrector higher order spectral method. While the method was intended as a means of reconstructing a given wave-field, it was also able to predict the free surface down-wave and into the future. The method, however, required high performance computation to properly solve the strongly nonlinear predictor-corrector problem. Hence, its calculation requirements are prohibitively expensive for real-time control of WECs. In a more real-time realisable method, Morris *et al.* (1992) and Halliday *et al.* (2011) used a discrete Fourier transform (both used the FFT algorithm) on a free surface measurement at a fixed location and attempted to predict the free surface down-wave by propagating the discretised Fourier components. They propagated these components by assuming they travelled at the phase velocity of linear water waves at the Fourier component’s bin frequency. The method was applied to synthetic unidirectional linear irregular waves. They found some modest success in predicting the free surface into the future in some circumstances, but equally poor predictions for others. While this work shows promise, further efforts are required to (i) apply such methods to experimental waves, (ii) provide quantitative details on how far down-wave or into the future the waves can be predicted (their results could show errors in the order of the significant wave height for various time or space forecasts), and (iii) detail why such a method should be valid other than assuming a sample’s discrete Fourier components are equivalent to the continuous spectrum of the underlying waves.

This work revisits the ideas of Morris *et al.* (1992) and Halliday *et al.* (2011) seeking to improve on these prior works by addressing points (i)-(iii). Contained within is a theoretical model for predicting irregular unidirectional waves using a discrete Fourier transform and linear water wave theory (a simplified, but potentially valid, way of forecasting the waves needed for active control of WECs). The prediction algorithm is examined within a rigorous mathematical framework in order to assess how waves can be forecast and is validated using experimental data.

Method Outline

Consider a field of irregular unidirectional surface gravity waves on a flat bed where waves propagate in the x -direction, the z -direction opposes gravitational acceleration $g = 9.81 \text{ m s}^{-2}$, and the distance between the equilibrium free surface and bed is H . Assume the waves are of low steepness such that they obey linear potential theory. The wave-field is therefore given as

$$\eta(x, t) = \text{Re} \left(\int_0^\infty A(\omega) e^{i(\omega t - k(\omega)x + P(\omega))} d\omega \right) = \text{Re} \left(\sum_{m=0}^\infty A_m e^{i(\omega_m t - k_m x + P_m)} \right), \quad (1)$$

where t is time, $A(\omega)$ is the amplitude spectrum (SI dimensions m s rad^{-1}), ω is angular frequency, k is the positive real root to the dispersion relation $k \tanh(kH) = \omega^2 g^{-1}$, and $P(\omega)$ is the phase

of each frequency component (which takes a random value uniformly distributed between $-\pi$ and π). The rightmost expression is defined for convenience where each m corresponds to an infinitesimal regular wave at a given frequency $\omega_m > 0$ with amplitude A_m and phase P_m .

Consider a free surface measurement device at location (without loss of generality) $x_A = 0$ that samples η for a finite duration $0 < t < \Delta T$ at a rate f_s (Hz). Let ΔT be the present time. Assume negligible wave energy above the Nyquist Frequency (which is $f_s/2$). By applying a discrete Fourier transform (e.g. the FFT) the free surface can be discretised as

$$\eta(x_A, t) = \text{Re} \left(\sum_{n=0}^N F(\omega_n) e^{i(\omega_n t)} \right) = \text{Re} \left(\sum_{n=0}^N \left(\sum_{m=0}^{\infty} F_m(\omega_n) \right) e^{i(\omega_n t)} \right), \quad \text{for } 0 < t < \Delta T, \quad (2)$$

where the ω_n 's are a set of finite frequencies, $F(\omega_n)$ is the (single sided and complex) results of the discrete transform, $N = (f_s \Delta T + 2)/2$, $\omega_{n+1} - \omega_n = \Delta\omega = (2\pi f_s)/(2N)$, and $F_m(\omega_n)$ is the (physically unobtainable) discrete Fourier transform of an m th wave component in equation 1. Note that the right hand side of equation 2 occurs because the Fourier transform is linear.

Although it is not physically obtainable, it is useful to consider the wave-field if each m th wave component could be transformed in isolation, which is

$$\eta(x_A, t) = \text{Re} \left(\sum_{m=0}^{\infty} \left(\sum_{n=0}^N F_m(\omega_n) e^{i(\omega_n t)} \right) \right), \quad \text{for } 0 < t < \Delta T. \quad (3)$$

As each m th wave component is, in essence, a regular wave, by assuming negligible discretisation errors the discrete Fourier transform of these components is given exactly by

$$\frac{\text{Re}(F_m)}{A_m} = \frac{\omega_m \sin(P_m) - \omega_m \sin(P_m + \omega_m \Delta T) \cos(\Delta T \omega_n) + \omega_n \cos(P_m + \omega_m \Delta T) \sin(\Delta T \omega_n)}{-0.5 \Delta T (\omega_m^2 - \omega_n^2)}, \quad (4)$$

$$\frac{\text{Im}(F_m)}{A_m} = \frac{\omega_m \sin(P_m + \omega_m \Delta T) \sin(\Delta T \omega_n) - \omega_n \cos(P_m) + \omega_n \cos(P_m + \omega_m \Delta T) \cos(\Delta T \omega_n)}{-0.5 \Delta T (\omega_m^2 - \omega_n^2)}. \quad (5)$$

Consider a down-wave location $x_B > x_A$ at a future time $t_B > \Delta T$. According to equations 1 and 3 this is given exactly by

$$\eta(x_B, t_B) = \text{Re} \left(\sum_{m=0}^{\infty} \left(\sum_{n=0}^N F_m(\omega_n) e^{i(\omega_n (t_B - c_m^{-1} x_B))} \right) \right), \quad (6)$$

if $0 < t_B - c_m^{-1} x_B < \Delta T$ for all m , where $c_m = \omega_m k_m^{-1}$ is the phase velocity of the m th wave component. In contrast, without changing any $F(\omega_n)$'s magnitude in equation 2, the only physically realisable way of predicting the free surface via a discrete Fourier transform is

$$\eta^P(x_B, t_B) = \text{Re} \left(\sum_{n=0}^N \left(\sum_{m=0}^{\infty} F_m(\omega_n) \right) e^{i(\omega_n t_n)} \right), \quad (7)$$

where t_n is a set of $N + 1$ 'seed times'. Optimally, the t_n 's should be selected to minimise the difference between $\eta(x_B, t_B)$ and $\eta^P(x_B, t_B)$. Hence, they are required to minimise the error, E , given by

$$E = \left| \text{Re} \left(\sum_{n=0}^N \sum_{m=0}^{\infty} F_m(\omega_n) \left(e^{i(\omega_n (t_B - c_m^{-1} x_B))} - e^{i(\omega_n t_n)} \right) \right) \right|. \quad (8)$$

The optimal choice of t_n therefore requires some *a priori* knowledge of $A(\omega)$ and $P(\omega)$. For example, if the waves are regular and it is known that $A = A_R \delta(\omega - \omega_R)$, the optimal choice is $t_n = t_B - c_R^{-1} x_B$ for all n . However, as this knowledge of $A(\omega)$ is unobtainable via finite time samples, it is proposed here that it is most pragmatic to set $t_n = t_B - c_n^{-1} x_B$, where c_n is the

phase velocity of the n th Fourier component's bin frequency. This is because, for a given A_m , $\text{Re}(F_m) + \text{Im}(F_m)$ is maximised near ω_n , and therefore the final term in equation 8 provides a good compromise between reducing the error for a given m th wave without substantially increasing the error for a different frequency wave. Similar reasoning requires that the prediction region is given as $0 < t_B - c_n^{-1}x_B < \Delta T$. Further mathematical analysis of t_n and the implications of equation 8 is beyond the scope of this abstract, but will be discussed at the Workshop. Nonetheless, it is therefore proposed that waves should be predicted as

$$\eta^P(x_B, t_B) = \text{Re} \left(\sum_{n=0}^N F(\omega_n) e^{i(\omega_n(t_B - c_n^{-1}x_B))} \right). \quad (9)$$

Prediction comparisons to experiments

The prediction algorithm was run using a range of JONSWAP spectra for significant wave heights of $H_s = 0.045, 0.085, 0.11, 0.15$ and 0.19 m, $\gamma = 3.3$, and with a peak frequency $\omega_p = 2.4 \text{ rad s}^{-1}$, which has corresponding peak wavelength $\lambda_p = 6.87$ m and peak period $t_p = 2.62$ s. The waves were generated in water of depth $H = 1.1$ m at the University of Western Australia's wave flume. They were measured using wave gauges spaced 5, 10, and 15 m apart, at a sampling rate of $f_s = 32$ Hz. The waves were generated for a minimum of 5 minutes and results analysed for the central 3 minutes. The spectra used in the experiments were considered because they are representative (excluding directionality) of Albany (Western Australia) wave conditions at 1/30th scale. This site is modelled because in the Summer of 2019/2020 Carnegie Clean Energy, who are actively pursuing real-time wave prediction for WEC control (Carnegie Clean Energy, 2018), intend on deploying their CETO6M there. The largest probe spacing allows waves to be predicted over 1.9 s in advance, which is the time required for the free surface to cause the excitation force on a 1/30th scale linear model of CETO6M (Falnes, 1995). The shorter spacings permit analysis of the algorithm with respect to distance. A beach was placed at the end of the flume, and post-processing found it reflected approximately 5% of the incident wave's energy. For all tests it was found that the results were invariant of $F(\omega_n)$ for $\omega_n < 0.25\omega_p = \omega_L$ and $\omega_n > 4\omega_p = \omega_U$. Hence, the transform was band-passed filtered by setting $F(\omega_n) = 0$ for $\omega_n < \omega_L$ and $\omega_n > \omega_U$.

Figure 1 shows the measured free surface signal for waves with $H_s = 0.11$ m and $\omega_p = 2.4 \text{ rad s}^{-1}$ overlaid with the prediction for the free surface there for $x_B/\lambda_p = 0.73$ and $t_B/t_p = 0.15$ as well as for $x_B/\lambda_p = 2.18$ and $t_B/t_p = 1.00$. Both predictions used $\Delta T/t_p = 10$. Note that for both of these simulations, the algorithm could produce the prediction in a time less than t_B ; emphasising the algorithm can predict waves in real time. Qualitatively, both prediction signals show pleasing agreement with the experimental signal. They have similar peaks, troughs, shapes, and distances between extrema. Neither prediction appears superior despite the dotted blue signal predicting waves at an increased time and distance. The biggest discrepancies occur around the peaks/troughs, and is likely the result of either reflections in the tank becoming more prominent or non-linear effects that are not included in the prediction model. These results are representative of all waves tested, however, as expected, larger H_s would result in increased discrepancies around peaks/troughs (presumably due to non-linear effects). The effect of varying H_s will be presented and discussed in greater detail at the workshop.

Figure 2 shows the time averaged root mean square error, \bar{L}_0 , between the prediction and measured signal with respect to the size of ΔT for waves with $H_s = 0.11$ m and $\omega_p = 2.4 \text{ rad s}^{-1}$. The leftmost figure shows the results of varying the prediction distance for a prediction time of $t_B/t_p = 0.15$ and the rightmost figure shows the results of varying the prediction time for a prediction distance of $x_B/\lambda_p = 2.18$.

In the leftmost figure, the algorithm's proposed prediction criteria (that $0 < t_B - c_n^{-1}x_B < \Delta T$ for all c_n given between the frequencies ω_L and ω_U) is only satisfied for $\Delta T/t_p > 3$ for the smaller x_B and for $\Delta T/t_p > 5$ for the larger x_B . When it is met, both predictions show an error of $\bar{L}_0/H_s \sim 0.06H_s$, wherein a smaller ΔT gives a slightly larger error, and an increasing $\Delta T/t_p$ beyond 10 does not improve the prediction. If this criteria is not met the prediction error is substantially larger. Interestingly, for $\Delta T/t_p > 10$, both prediction distances give sim-

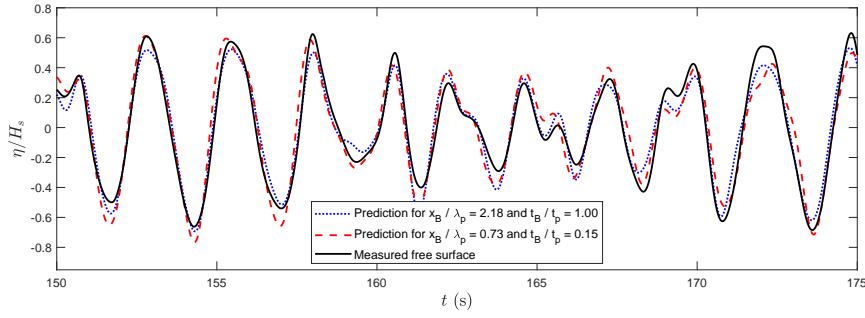


Figure 1: Comparison between predicted free surface and measured free surface for waves with $H_s = 0.11$ m and $\omega_p = 2.4$ rad s $^{-1}$ with prediction algorithm using $\Delta T/t_p = 10$.

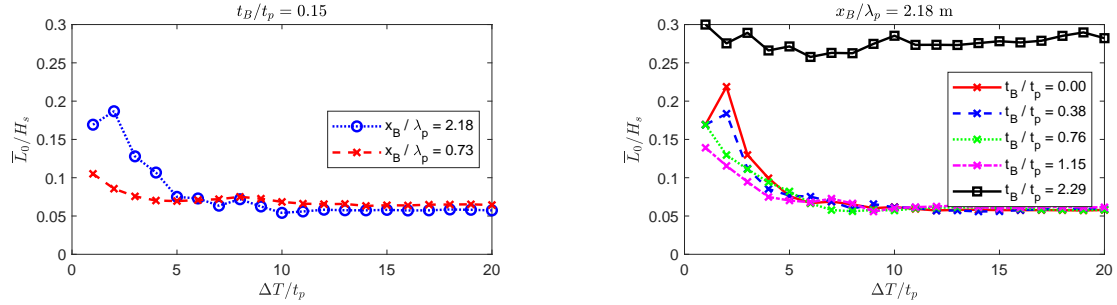


Figure 2: The \bar{L}_0 error between experimental measurement and prediction with respect to the algorithm's ΔT for waves with $H_s = 0.11$ m and $\omega_p = 2.4$ rad s $^{-1}$. Left: Comparing errors of prediction distances for $t_B/t_p = 0.15$. Right: Comparing errors of prediction times over prediction distance $x_B/\lambda_p = 2.18$.

ilar errors (differences $< 0.005H_s$), which indicates that over small distances the soundness of the prediction is not affected by the distance of the prediction; although the accuracy of the prediction is fundamentally limited. In the rightmost figure the proposed prediction criteria is valid for $\Delta T/t_p > 8$ for all curves except the $t_B/t_p = 2.29$ curve (solid black with squares), which does not satisfy the prediction criteria anywhere. For all curves except the solid black the error converges to $\sim 0.06H_s$ for $\Delta T/t_p > 8$, however, the solid black never converges and always gives errors $> 0.25H_s$. In conjunction with the leftmost figure, this implies that, provided the prediction is made within the well-defined region $0 < t_B - c_n^{-1}x_B < \Delta T$ for all c_n given between frequencies ω_L and ω_U , the algorithm is capable of predicting times in the order of the peak wave period, distances in the order of the peak wavelength, and is therefore capable of predicting waves for real-time control of a WEC in unidirectional low steepness seas.

Acknowledgements

This research was conducted by the Wave Energy Research Centre and jointly funded by the University of Western Australia and the Western Australian Government, via the Department of Primary Industries and Regional Development (DPIRD).

References

- BABARIT, A. & CLÉMENT, A. H. 2006 Optimal latching control of a wave energy device in regular and irregular waves. *Applied Ocean Research* **28** (2), 77–91.
- CARNEGIE CLEAN ENERGY 2018 CETO and Albany Update. <https://s3-ap-southeast-2.amazonaws.com/website-sydney-1/media/2018/09/21122414/19-09-21-CETO-and-Albany-Update.pdf>.
- FALNES, J. 1995 On non-causal impulse response functions related to propagating water waves. *Applied Ocean Research* **17** (6), 379–389.
- HALLIDAY, J. R., DORRELL, D. G. & WOOD, A. R. 2011 An application of the Fast Fourier Transform to the short-term prediction of sea wave behaviour. *Renewable Energy* **36** (6), 1685–1692.
- MORRIS, E. L., ZIENKIEWICZ, H. K., POURZANJANI, M. M. A., FLOWER, J. O. & BELMONT, M. R. 1992 Techniques for sea state prediction. In *2nd International Conference on Maneuvering and Control of Marine Craft*, pp. 547–571. Southampton, UK.
- QI, Y., WU, G., LIU, Y., KIM, M. & YUE, D. K. P. 2018 Nonlinear phase-resolved reconstruction of irregular water waves. *Journal of Fluid Mechanics* **838**, 544–572.
- RINGWOOD, J. V., BACELLI, G. & FUSCO, F. 2014 Energy-maximizing control of wave-energy converters: The development of control system technology to optimize their operation. *IEEE Control Systems* **34** (5), 30–55.